

NASA-CR-197605

(NASA-CR-197605) SIMULATION OF
WAVE PROPAGATION IN
THREE-DIMENSIONAL RANDOM MEDIA
(California Univ.) 31 p

N95-19547

Unclas

G3/32 0038411

Dec. 16, 1993

Simulation of wave propagation in three-dimensional random media

Wm. A. Coles and J. P. Filice*

*Electrical and Computer Engineering
University of California, San Diego, CA 92093-0407*

R. G. Frehlich, and M. Yadlowsky†

*Cooperative Institute for Research in the Environmental Sciences (CIRES)
University of Colorado, Boulder, CO 80309*... N.A. 68-253
38411
p. 31

Abstract

Quantitative error analysis for simulation of wave propagation in three dimensional random media assuming narrow angular scattering are presented for the plane wave and spherical wave geometry. This includes the errors resulting from finite grid size, finite simulation dimensions, and the separation of the two-dimensional screens along the propagation direction. Simple error scalings are determined for power-law spectra of the random refractive index of the media. The effects of a finite inner scale are also considered. The spatial spectra of the intensity errors are calculated and compared to the spatial spectra of intensity. The numerical requirements for a simulation of given accuracy are determined for realizations of the field. The numerical requirements for accurate estimation of higher moments of the field are less stringent.

1. Introduction

To analyze the propagation of waves in random media one normally writes equations for the propagation of the statistics of the field (such as the moments). In the case of small-angle forward-scattering the differential equations for the propagation of the higher field moments are difficult to solve. Consequently one must make various approximations, such as the Born and Rytov weak-scattering approximations or the Gaussian-field strong-scattering approximation. In fact moments higher than the fourth are so difficult that no solutions are known outside of the asymptotic weak and strong approximations. Frequently, then, it is necessary to solve the equations by numerical methods.

*Now at Photon Research Associates, San Diego

†Now at BEIP, National Institute of Health, Bethesda, MD, 20892

In a numerical simulation, by contrast, one generates a realization of the random medium (which has the desired statistics) and calculates the resulting wave field. It is actually a numerical experiment rather than a numerical analysis. The desired statistic of the wave field can then be estimated by repeating the experiment until the estimation errors are satisfactory. The simulation lies conceptually between an experiment and an analysis and it offers some unique benefits.

A single set of simulations will provide all the statistics of the field that are of interest, whereas for theoretical and numerical analysis, each statistic must be considered separately. This is particularly useful for higher moments or more complex field statistics. It is easy to change the statistics of the medium and repeat a set of simulations, whereas the calculation might require a completely different set of approximations. Furthermore a simulation is an excellent check for the sort of errors than can easily occur in a complex analysis.

A simulation cannot, of course, replace an experiment; but it can help identify the important factors in the experiment. For example if the medium is turbulent it is very difficult to generate or even to identify periods of uniform homogeneous turbulence. Generally real turbulent processes are non-stationary and inhomogeneous in a way which is described as intermittent. It is often very difficult to measure the appropriate statistics of the medium and usually impossible to thoroughly sample the region of interest. Thus when an experiment disagrees with a theoretical calculation it is difficult to tell if the calculation is at fault or if the statistical model of the medium is inadequate. Simulations have been used to resolve disagreements between theoretical predictions and experiments¹. Simulations have recently been used to investigate the effects of intermittency on laser propagation by Frehlich². These issues are important for predictions of the effects of refractive turbulence on coherent lidar^{3,4}.

Another case of interest occurs when it is impossible to observe the process long enough to obtain an ensemble average. This is quite often the case in astronomical observations of scattering in the interstellar medium. Here one might wish to know if some feature of the observation is due to a peculiarity of the medium (i.e. something deterministic) or if it is simply a chance sample from a homogeneous stochastic process. Indeed one may find it very difficult to describe the feature in question in terms of moments of the random field. In a simulation one can compare the wave field with the realization of the random medium in a point by point manner. This approach was used by Coles and Filice⁵ to demonstrate the effect of refraction by large scale structures on the dynamic spectra of intensity scintillation in the solar wind.

Simulations of wave propagation through a thin phase-screen with only one transverse dimension have been widely used in the study of ionospheric propagation, where the statistics are believed to be highly anisotropic⁶⁻¹¹. Simulations of radio propagation through the solar-wind use the phase-screen approximation with two transverse dimensions^{5,12}. However in nearly isotropic media, such as the atmosphere, a three-dimensional simulation (two transverse dimensions and one propagation dimension) is clearly necessary. These are more demanding of computational resources (both memory and processor) and much more care must be given to the effect of the computational mesh on the accuracy of the result. These issues appear to have been first investigated by Filice¹²; they have also been discussed qualitatively by Martin and Flatte^{13,14}. A review of simulation of wave propagation in random media is presented by Martin¹⁵. For extended random media, Spivack and Uscinski¹⁶ presented the leading order error scaling for the field and second moment as a function of the

separation between the screens Δz for simulations in a random medium with one transverse dimensions (two-dimensional simulation).

The purpose of this paper is to present quantitative results for the optimal choice of the mesh size for simulation of wave propagation through a three-dimensional random medium. The propagation problem we consider is small-angle forward-scattering by a phase changing medium. The refractive index of the medium is a three-dimensional Gaussian random process $n(\vec{r})$ which is completely described by its structure function $D_n(\vec{r})$ or its spatial power spectrum $\Phi_n(\vec{q})$. The notation of Prokhorov et al¹⁷ will be used throughout. We have investigated power-law processes with structure functions of the form $D_n(\vec{r}) = C_n^2 r^{\alpha-1}$. For such processes the spatial power spectrum is

$$\Phi_n(q) = A(\alpha) C_n^2 q^{-\alpha-2} \quad \text{where} \quad A(\alpha) = \Gamma(\alpha + 1) \sin[(\alpha - 1)\pi/2]/4\pi^2. \quad (1)$$

Much of the application of this work is to turbulent media with high Reynolds number in which an inner-scale is important. To investigate the effect of the inner-scale l_o on simulation error we used the universal spectrum for the Kolmogorov exponent $\alpha = 5/3$

$$\Phi_n(q) = 0.0330054 C_n^2 q^{-11/3} f(q l_o) \quad \text{where} \quad f(x) = (1 + a_1 x + a_2 x^2 + a_3 x^3) \exp(-x). \quad (2)$$

We used $a_1 = 1.4284$, $a_2 = 1.1987$, $a_3 = 0.1414$, as estimated from laser scintillation data by Frehlich¹⁸. We have studied three geometries: a plane wave normally incident on a thin slab of random medium; a plane wave normally incident on a half-space of uniform homogeneous random medium; and a point source embedded in a uniform homogeneous medium. The thin slab or screen problem is a canonical case because the extended medium can be treated as a stack of slabs.

2. Forward Scattering Theory

The choice of computational mesh depends on the important spatial scales in the random field in the observation plane. Here we will review the forward scattering theory necessary to estimate these scales. If the scattering angle is small it is convenient to write the field with respect to a monochromatic plane wave as $F(\vec{s}, z, t) = f(\vec{s}, z) \exp[i(kz - \omega t)]$. Here \vec{s} is the transverse coordinate and $k = 2\pi/\lambda$. The intensity is defined as $I(\vec{s}, z) = \langle f(\vec{s}, z) f^*(\vec{s}, z) \rangle$. It is also useful to normalize the field so that the average intensity $\langle I(\vec{s}, z) \rangle$ is unity. This leads to the parabolic wave equation

$$\frac{\partial f}{\partial z}(\vec{s}, z) = \frac{i}{2k} \nabla_t^2 f(\vec{s}, z) + i k n(\vec{s}, z) f(\vec{s}, z), \quad (3)$$

where ∇_t is the transverse gradient operator and $n(\vec{r})$ is the deviation of the refractive index from its mean value.

Propagation equations for the moments of the field can be derived under the Markov approximation^{19,20}. This is equivalent to the assumption that the continuous random medium can be decomposed into a series of statistically independent thin slabs. These slabs must be sufficiently thin that each acting alone would cause only small phase fluctuations. The conditions for the validity of this approximation have been determined for the first moment or average field, the second moment or mutual coherence function, and the

fourth moment²⁰. The conditions for the validity of the second and fourth moment are very weak and for isotropic turbulence essentially equivalent to the small-angle approximation of the parabolic equation. We will also make this approximation in the numerical simulation; although it is not essential it greatly simplifies the calculations.

The propagation of the second field moment or mutual coherence function $\Gamma_2(\vec{x}_1, \vec{x}_2) = \langle f(\vec{x}_1)f^*(\vec{x}_2) \rangle$ admits an analytical solution for the cases of interest here. If the field is wide sense stationary (i.e. Γ_2 is only a function of $\vec{s}_{12} = \vec{x}_1 - \vec{x}_2$) then the Fourier transform of Γ_2 is the spatial power spectrum of the field. The bandwidth of this power spectrum sets the required sampling interval. The propagation equation for $\Gamma_2(\vec{x}_1, \vec{x}_2)$ is given by Prokhorov et al,¹⁷ in terms of $D'(\vec{s}, z)$, the longitudinal gradient of the wave structure function

$$\frac{\partial \Gamma_2}{\partial z}(\vec{x}_1, \vec{x}_2, z) = \frac{i}{2k}(\nabla_1^2 - \nabla_2^2)\Gamma_2 - \frac{1}{2}D'(\vec{s}_{12}, z)\Gamma_2(\vec{x}_1, \vec{x}_2, z) \quad (4)$$

$$D'(\vec{s}, z) = 4\pi k^2 \int \int_{-\infty}^{\infty} d^2q [1 - \cos(\vec{q} \cdot \vec{s})] \Phi_n(\vec{q}, q_z = 0, z). \quad (5)$$

In the planar geometry the term $(\nabla_1^2 - \nabla_2^2)\Gamma_2$ is identically zero and the solution at range R can be written

$$\Gamma_2(\vec{s}, R) = \exp[-\frac{1}{2}D_P(\vec{s}, R)] \quad (6)$$

where

$$D_P(\vec{s}, R) = \int_0^R dz D'(\vec{s}, z). \quad (7)$$

A similar solution applies for a spherical wave if $D_P(\vec{s}, R)$ is replaced by

$$D_S(\vec{s}, R) = \int_0^R dz D'(\vec{s}z/R, z). \quad (8)$$

The wave structure functions $D_P(\vec{s})$ and $D_S(\vec{s})$ can also be written as $D(\vec{s}) = \langle [\phi(\vec{r}) - \phi(\vec{r} + \vec{s})]^2 \rangle$ where $\phi(\vec{r})$ is the phase on a geometrical path from the source to the receiver. So $D(\vec{s})$ is a measure of the differential phase variance on a baseline \vec{s} . The field coherence scale s_o can be defined by $D(s_o) = 1$. This scale s_o is inversely related to the rms scattering angle because the Fourier transform of $\Gamma_2(\vec{s})$ is the spatial spectrum $\Gamma_2^t(\vec{q})$. A component of the spatial spectrum at frequency \vec{q} corresponds to a plane wave propagating at an angle of $\theta = \sin^{-1}(q/k)$ to the z axis. Thus the width of the angular spectrum can be defined as $\theta_o = 1/(ks_o)$.

The propagation equation for the fourth moment of the field $\Gamma_4 = \langle f(\vec{x}_1) f^*(\vec{x}_2) f(\vec{x}_3) f^*(\vec{x}_4) \rangle$ is

$$\frac{d\Gamma_4}{dz} = \frac{i}{2k}(\nabla_1^2 - \nabla_2^2 + \nabla_3^2 - \nabla_4^2)\Gamma_4 - V\Gamma_4 \\ 2V = D'(\vec{s}_{12}) + D'(\vec{s}_{14}) + D'(\vec{s}_{23}) + D'(\vec{s}_{34}) - D'(\vec{s}_{13}) - D'(\vec{s}_{24}). \quad (9)$$

The case of greatest interest is when $\vec{s}_{12} = \vec{s}_{34} = 0$. Then $\Gamma_4 = \langle I(\vec{r})I(\vec{r} + \vec{s}_{13}) \rangle = 1 + C_I(\vec{s}_{13})$ where $C_I(\vec{s}_{13})$ is the covariance of the intensity fluctuations. This can be solved

in weak scattering using the Born approximation and in strong scattering using various series expansions (none of which converge quickly). Solutions for pure power-law and for Gaussian spectra of refractive index have been summarized by Prokhorov et al.¹⁷. Solutions for power-law spectra with inner scales have been given by Fante²¹ for the case of a plane wave incident on a homogeneous half space and by Frehlich²² for the case of a point source embedded in a homogeneous medium. The most important characteristics of the intensity covariance are outlined below for power-law and related spectra.

For weak scattering the intensity variance $m^2 = C_I(0)$ is less than unity and the shape of $C_I(\vec{s})$ is independent of the level of the refractive index spectrum, but the variance m^2 is linearly proportional to this level. In weak scattering the spatial scale of $C_I(\vec{s})$ is the radius of the first Fresnel zone $r_f = (R/k)^{0.5}$ when the inner scale is less than the Fresnel scale, otherwise it is proportional to the inner scale. The Born variance is $m_b^2 = KD(r_f)$ where K is a constant of the order of unity which depends weakly on the shape of the spectrum and the incident wave (e.g. equations 26 and 38). The Born variance m_b^2 is a useful measure of the strength of scattering even when $m_b^2 \gg 1$, that is when m_b^2 is not a good approximation to m^2 .

In strong scattering as $m_b^2 \rightarrow \infty$, the field approaches a (complex) Gaussian process, the mean field approaches zero, and the intensity covariance approaches $C_I(\vec{s}) = \exp[-D(\vec{s})]$, i.e. the intensity has unit variance and spatial scale (at $1/e$) of s_o . The first correction to this strong scattering limit adds two terms to $C_I(\vec{s})$; $C_r(\vec{s})$ and $C_{dr}(\vec{s})$. It is conceptually helpful to model the intensity as a diffractive process of scale s_o modulated by a refractive process of larger scale s_r ²³. If $D(\vec{s})$ is isotropic the scale of the refractive process is the distance subtended by the scattering angle, that is $s_r = \theta_o R$. The product term is $C_{dr}(\vec{s}) = \exp[-D(\vec{s})]C_r(\vec{s})$. Thus C_r and C_{dr} carry equal variance, but, as C_r is of much larger scale, the scale of C_{dr} is approximately s_o . If $D(\vec{s})$ is anisotropic the refractive process is also anisotropic with the same axial ratio, but not, as one might expect, of the form $\vec{\theta}_o R$. Rather, the minor axis of \vec{s}_r is equal to the major axis of $\vec{\theta}_o R$ ²⁴.

Three important scales emerge from the analysis of the second and fourth moments. The first is the field coherence length s_o . The second is the scattering disc $\theta_o R$. The third is the radius of the first Fresnel zone r_f . The three scales are not independent as $r_f^2 = s_o s_r$. Fortunately these scales can be determined from the geometry and the analytical solution for the second moment.

3. The Propagation Calculation

The propagation of a wave through a random medium according to the parabolic wave equation is the limiting case of propagation through a series of discrete phase screens separated by free space. A finite number of screens N_S can be used if the phase fluctuations in each screen are small. However the simulation of this problem is greatly assisted if these screens are statistically independent. This decomposition into independent weak phase screens is equivalent to the Markov approximation which is usually made when such problems are solved analytically. The effects of correlated screens on simulations with one transverse dimension was shown to be small¹⁶ when the separation between screens was larger than the correlation distance of the refractive index fluctuations. Clearly it is possible to simulate a medium in which the Markov approximation breaks down and this would be an interesting

project. However in the work reported here we have used independent screens.

The passage of a wave $f(\vec{s}, z)$ through a thin screen with phase fluctuations $\phi(\vec{s})$ at $z=0$ can be expressed as $f(\vec{s}, 0^+) = f(\vec{s}, 0^-) \exp[i\phi(\vec{s})]$. The propagation between the screens in free-space is expressed as a convolution using the Fresnel integral. For numerical work it is efficient to do the convolution in the Fourier transform domain using the Fast Fourier Transform (FFT) algorithm (i.e. $f^t(\vec{q}, z) = f^t(\vec{q}, 0) \exp[-izq^2/(2k)]$ where $f^t(\vec{q}, z)$ is the Fourier transform of $f(\vec{s}, z)$).

The simulation begins by generating a series of independent phase screens $\phi_n(\vec{s})$ for $n = 1, \dots, N_S$ separated by Δz . The field incident on the first screen is deterministic. The field incident on a screen $f(\vec{s}, n\Delta z^-)$ is propagated to the next by: multiplying the incident wave by the phase transmittance $\exp[i\phi_n(\vec{s})]$; Fourier transforming the field; multiplying the transform by the free space propagator $\exp(-iq^2\Delta z/2k)$; and finally retransforming to obtain the field incident on the next screen. That is

$$f[\vec{s}, (n+1)\Delta z^-] = Ft^{-1}\{Ft[f(\vec{s}, n\Delta z^-) \exp(i\phi_n(\vec{s}))] \exp[-iq^2\Delta z/(2k)]\}. \quad (10)$$

The field is a bandlimited random process and we can use sampling theory to choose the appropriate grid spacing. In general a field of propagating waves is strictly bandlimited because $q \leq k$. Thus the original field can be reconstructed from samples taken at intervals of $\Delta s \leq 2\pi/(2k) = \lambda/2$ without any loss of information. In this case we are considering only small angle forward scattering so the field is actually bandlimited much more severely. In fact the spatial spectra of interest typically have a form similar to $\exp(-q^2/q_0^2)$. Thus there is no significant power for $q > q_{max}$, where $q_{max} \approx 3q_0$. Then a sample interval of $\Delta s \approx \pi/q_{max} \approx s_0$ will be adequate.

The grid must be of finite extent and the characteristics of the Discrete Fourier Transform (DFT) imposes periodicity of the fields. In choosing this period we are guided by the characteristics of the angular spectrum and the intuitive interpretation of the rigorous path-integral solution for the fields. In weak scattering (when the Born approximation holds) the field in the observation plane is determined primarily by the scattering medium inside the first Fresnel zone of rays²⁵ because these contributions arrive in-phase. The maximum extent of the first Fresnel zone is given by r_f . In strong scattering the components of the scattered field are more randomly phased. In this case, the important region of scattering is not the first Fresnel zone but the radius of the scattering disc $\theta_0 R$ which is defined by the angular spectrum. The scattering disc is larger than the first Fresnel zone if $r_f > s_0$. This implies $D(r_f) > 1$ which is consistent with other definitions of strong scattering based on the intensity variance. As it happens the largest scale of the random field (s_r) is the radius of the scattering disc so the screen size is also appropriate for the receiving plane. If spatial statistics are desired, as is normally the case, then the screen must be large enough that each point of interest is at least $\theta_0 R$ away from the edge of the screen. A similar argument based on the spatial intensity spectrum has been used to estimate the required screen dimensions¹³⁻¹⁵. We use a square screen of dimensions $\approx 4\theta_0 R$. A rectangular screen was also used for comparison.

4. Generation of a Random Screen

The thin slab of random medium in $-\Delta z/2 < z < +\Delta z/2$ is described by the spatial spectrum of refractive index fluctuations $\Phi_n(\vec{q}, z)$. The two-dimensional phase fluctuations $\phi(\vec{s}, z)$ are given by

$$\phi(\vec{s}, z) = k \int_{-\Delta z/2}^{+\Delta z/2} dz n(\vec{s}, z). \quad (11)$$

The two-dimensional spatial spectrum of phase fluctuations under the Markov approximation is

$$\Phi_\phi(q_x, q_y, z) = 2\pi k^2 \Delta z \Phi_n(q_x, q_y, q_z = 0, z). \quad (12)$$

The random phase screen is represented as a set of real numbers $\{\phi_{mn}\}$ which are samples of a continuous random process $\phi(\vec{s})$ over a finite range. The process $\phi(\vec{s})$ is a member of an ensemble with power spectral density $\Phi_\phi(\vec{q})$. The sample interval is $\Delta x, \Delta y$ and the simulation dimension is L_x, L_y . The $\{\phi_{mn}\}$ are generated in the frequency domain from a set of complex random numbers $\phi_{pq}^t = A_{pq} + iB_{pq}$. Here A_{pq} and B_{pq} are independent zero-mean Gaussian random variables both with variance

$$\sigma_{pq}^2 = \langle |\phi_{pq}^t|^2 \rangle = \frac{4\pi^2 MN}{\Delta x \Delta y} \Phi_\phi(2\pi p/L_x, 2\pi q/L_y). \quad (13)$$

The Gaussian random numbers A_{pq} and B_{pq} are generated from a pair of uniformly distributed random numbers using the Box-Muller transformation. Realizations of the phase $\{\phi_{mn}\}$ are obtained from the DFT of $\{\phi_{pq}^t\}$. The real and imaginary parts of ϕ_{mn} are uncorrelated and represent realizations of the desired random process, i.e., the expectation of the respective sample spectra are $\Phi_\phi(\vec{q})$. The continuous sample spectrum is

$$\begin{aligned} C_\phi(\vec{q}) &= \frac{1}{L_x L_y} \left| \int_0^{L_x} \int_0^{L_y} \phi(\vec{s}) \exp(-i\vec{q} \cdot \vec{s}) d^2 s \right|^2 \\ &= \frac{(\Delta x \Delta y)^2}{L_x L_y} \left| \sum_0^M \sum_0^N \phi_{mn} \exp[-i(q_x m \Delta x + q_y n \Delta y)] \right|^2. \end{aligned} \quad (14)$$

The discrete sample spectrum is then

$$C_\phi(2\pi p/L_x, 2\pi q/L_y) = \frac{(\Delta x \Delta y)^2 |\phi_{pq}^t|^2}{L_x L_y 4\pi^2} = \frac{\Delta x \Delta y}{MN} \frac{|\phi_{pq}^t|^2}{4\pi^2} \quad (15)$$

and substitution of Eq. (13) in (15) demonstrates that $\langle C_\phi(\vec{q}) \rangle = \Phi_\phi(\vec{q})$ as required.

5. Plane Wave Incident on a Thin Phase Screen

We tested the canonical problem of the plane wave incident on a thin phase screen using the universal power-law spectrum given in Eq. (2) for the phase spectrum, i.e.,

$$\Phi_\phi(\vec{q}) = T q^{-\alpha-2} f(q l_0) \quad (16)$$

where $T = 2\pi k^2 A(\alpha) C_n^2 \Delta z$. For a pure power-law spectrum ($l_0 = 0$) and for $0 < \alpha < 2$, the strength of scattering m_b^2 , the coherence scale s_o and the structure function $D_{TS}(\vec{s})$ are given by

$$m_b^2 = 4\pi T \Gamma(1 - \alpha/2) \cos(\alpha\pi/4) r_f^\alpha / \alpha = K_1(\alpha) D_{TS}(r_f) \quad (17)$$

$$K_1(\alpha) = 2^\alpha \Gamma(1 + \alpha/2) \cos(\alpha\pi/4) \quad (18)$$

$$D_{TS}(\vec{s}) = (s/s_o)^\alpha = 4\pi T \frac{\Gamma(1 - \alpha/2)}{\alpha \Gamma(1 + \alpha/2)} (s/2)^\alpha. \quad (19)$$

We have argued that the sample interval $(\Delta x, \Delta y)$ should be of the order of the coherence scale s_o and that the screen size should be of the order of the scattering disc $\theta_o R$. The coherence scale decreases with increasing strength of scattering and the scattering disc increases. Thus the memory and computation time required increase very rapidly with increasing strength of scattering. It is important to establish the strongest scattering that can be simulated with a specified error.

A reference calculation of was performed using a 2048×2048 point array with $\Delta x = \Delta y = r_f/64$ and $L_y = L_x = 64r_f$. The effect of the finite sample interval or sampling error was estimated by resampling the reference screen at $\Delta x = \Delta y = r_f/32, r_f/16, r_f/8$ and $r_f/4$, recalculating the field for each resampled screen, and comparing the results of each resampled calculation with the reference calculation. For all cases studied the rms error of the real part of the field was equal to the rms error of the imaginary part of the field and both were half the rms error of the intensity I_{rms} . These tests were done for two exponents ($\alpha = 1$ and $5/3$) and three strengths of scattering ($m_b^2 = 0.1, 1$ and 10).

The error for a pure power-law spectrum should depend only on $\Delta s/s_o$ because the shape of the spectrum does not depend on the strength of scattering. We tested this by plotting I_{rms} versus $\Delta s/s_o$ in Fig. 1. The error was well described by power-law model, [$I_{rms} = 0.671(\Delta s/s_o)^{0.514}$ for $\alpha = 1$ and $I_{rms} = 0.382(\Delta s/s_o)^{0.875}$ for $\alpha = 5/3$]. Since the error is caused by aliasing it should be a steeper function of $\Delta s/s_o$ for steeper spectra. Indeed we find (approximately) that $I_{rms} \propto (\Delta s/s_o)^{\alpha/2}$. We also find that there is essentially no change in the rms intensity m_{dec} as Δs increases, even when the intensity error I_{rms} is equal to m_{dec} . If we write the intensity of the resampled screen as $I_{dec} = I + \Delta I$ then

$$m_{dec}^2 = Var(I + \Delta I) = m^2 + I_{rms}^2 + Cov(I, \Delta I) \quad (20)$$

where $Cov(I, \Delta I) = \langle (I - 1)\Delta I \rangle$ is the covariance of I and ΔI . Clearly then the sampling error ΔI is anti-correlated with the intensity I , i.e. as Δs increases I_{dec} tends to underestimate the intensity peaks and overestimate the intensity nulls. This is exactly the behavior one expects of a low-pass filter.

We also simulated three cases with an exponent of $\alpha = 5/3$ and an inner scale of $l_o = 5\Delta s$. These examples were normalized to the pure power-law case with $\alpha = 5/3$ by setting the spectral levels the same at low wavenumber. For this test the spectrum changes with the sample interval so I_{rms} should not be expected to scale as $\Delta s/s_o$. The results are displayed in the bottom panel of Fig. 1. As one would expect, when $\Delta s > l_o$ the result is the same as

for the pure power-law case. When $\Delta s < l_o$ the error is much less than the pure power-law case because the spectrum drops faster at high frequencies and the effects of aliasing are greatly reduced. As for the pure power-law spectra, there is essentially no change in the rms intensity m_{dec} , even for I_{rms} equal to m_{dec} .

The spatial spectrum of intensity fluctuations $\Phi_I(q)$ for $m_b^2 = 10$ and a pure power-law phase spectrum ($\alpha = 5/3$) is shown in Fig. 2. The spectra of the intensity error ΔI for $\Delta s = r_f/32$ and $r_f/16$ are overplotted as open symbols. It is interesting to see that the sampling errors are almost white, i.e. the errors are independent. These errors are caused by aliasing in the angular spectrum, so they are introduced near the Nyquist frequency, however after the propagation calculation they have spread almost uniformly throughout the intensity spectrum.

The errors introduced by the finite dimensions of the simulation or windowing errors are more difficult to investigate. The random screen generated using the DFT is periodic. Originally we created a large reference screen and calculated a reference field. Then we reduced the window by truncating the reference screen. However the errors calculated this way increased much more rapidly than we expected (i.e. $I_{rms} \propto L_y/s_r$). The problem is clearly that the truncation process removes the periodicity in the screen and the discontinuities at the edges of the simulation produce additional errors that increase as the observation point approaches the edge of the simulation. This additional error would not exist if the screen had been generated at the smaller size.

The windowing error is more easily examined in the transform domain. The propagation algorithm conserves power so, with our field normalization, the mean intensity in any observing plane is exactly unity. The intensity spectrum is estimated by the DFT so its dc component is also exactly unity. However the dc component of the DFT should have included the integral over the resolution cell centered on the origin. Thus we have made an error in the spectrum which causes an error in the variance, which can be approximated as

$$\Delta m^2 = \int_{-2\delta\pi/L_x}^{2\delta\pi/L_x} dq_x \int_{-2\delta\pi/L_y}^{2\delta\pi/L_y} dq_y \Phi_I(q_x, q_y) \quad (21)$$

where δ is the fraction of the zero-frequency bin that is incorporated into the DC component. This error is easily estimated because the integration is confined to very low frequencies ($q < 2\pi/L$) and a low frequency approximation to the intensity spectrum is known^{17,26}.

$$\Phi_I(q) = 4\Phi_\phi(q) \sin^2[q^2 R/(2k)] \exp[-D_{TS}(qR/k)] \quad (22)$$

If we choose $L > \pi\theta_o R$, as we have argued intuitively, then the arguments of both the exponential and the \sin^2 term are small and one can do a power series expansion. The integral can then be done term by term. The first term, if $L_x = L_y$, is

$$\frac{\Delta m^2}{m_b^2} = \frac{\alpha(2\pi\delta r_f/L)^{4-\alpha} I(\alpha)}{\pi \cos(\pi\alpha/4)\Gamma(1-\alpha/2)} \quad (23)$$

where

$$I(\alpha) = \int_0^1 dx \int_0^1 dy (x^2 + y^2)^{1-\alpha/2} \quad (24)$$

and $I(5/3) = 0.89627$. An example of the windowing error for the pure Kolmogorov spectrum with $m_b^2 = 1.0$ is plotted in Fig. 3. Here m^2 is displayed in the upper panel and $\Delta m = [m_{ref}^2 - m^2]^{1/2}$ is displayed in the lower panel, to permit comparison with the sampling error I_{rms} . The theoretical model [Eqs. (21), (22) and $\delta = 0.65$] is a dashed line and the best-fit power-law function is the solid line. Clearly both fit adequately in the range of interest.

These calculations confirm our intuitive expectation that the sample interval should be a fraction of the coherence scale and that the window should be larger than the scattering disc. Since the scattering disc is inversely proportional to the coherence scale the number of points on the x and y axes must be $N \propto \theta_o R/s_o \propto 1/s_o^2$. For a power-law spectrum of exponent α the coherence scale $s_o \propto (m_b^2)^{-1/\alpha}$. Therefore the number of points needed is $N_{p2} \propto (m_b^2)^{4/\alpha}$.

6. Plane Wave Incident on a Uniform Medium

The simulation of an extended medium is performed by collapsing slabs of random media with thickness Δz into a series of N_S thin weak phase screens as discussed before. The sample mesh for each screen must be chosen so $\Delta y \approx 2r_f/\sqrt{N}$ and $L_y \approx 2r_f\sqrt{N}$. The remaining question is how to choose Δz the screen spacing.

For a pure power-law spectrum ($l_0 = 0$) and for $0 < \alpha < 2$, the strength of scattering m_b^2 , the coherence scale s_o and the structure function $D_P(\vec{s})$ are given by²²

$$m_b^2 = K_2(\alpha)D_P(r_f) \quad (25)$$

$$K_2(\alpha) = 2^{\alpha+1}\Gamma(1 + \alpha/2)\cos(\alpha\pi/4)/(2 + \alpha) \quad (26)$$

$$D_P(\vec{s}) = (s/s_o)^\alpha = B_1(\alpha)k^2C_n^2Rs^\alpha \quad (27)$$

$$B_1(\alpha) = 2^{1-\alpha}\Gamma(\alpha)\Gamma(1 - \alpha/2)\sin[(\alpha - 1)\pi/2]/\Gamma(1 + \alpha/2). \quad (28)$$

For the Kolmogorov exponent, $B_1(5/3) = 2.91438$ and $K_2(5/3) = 0.421602$. The strength of each phase screen is given by Eq. (16) as $T = 2\pi k^2 A(\alpha)C_n^2\Delta z$. After the field has propagated a distance Δz , the perturbation of the field introduced by the phase screen must be small. Because the field incident on the phase screen is random, a rigorous estimate of the magnitude of the field perturbation is difficult. A simple estimate of the magnitude of the field perturbation is the Born variance m_b^2 [Eq. (17)]. This implies that $\Delta z \propto 1/m_b^2$.

The extended medium simulation was tested against a reference as before. The reference mesh was $\Delta x = \Delta y = \Delta s = r_f/16$, $\Delta z = R/N_S$. We generated $N_S = 128$ independent 512×512 random phase screens and calculated the field in the receiving plane. The screen spacing was then doubled by summing pairs of screens, the field was recalculated and the rms intensity error was determined by comparison with the reference field. This procedure was repeated to obtain the intensity errors for $\Delta z/R = 1/N_S = 1/64, 1/32, 1/16$ and $1/8$. The rms intensity error is plotted as a function of $\Delta z/R$ in Fig. 4. The estimation error of each point is less than the size of the symbol. For a fixed m_b^2 and pure power-law spectra,

I_{rms} has a power-law dependence. It is interesting that I_{rms} is larger for flatter spectra, and also changes more slowly with Δz , clearly the high spatial frequency components are dominating the intensity errors. For the Kolmogorov exponent $\alpha = 5/3$, the collection of Δz errors follow an approximate scaling rule $I_{rms}^2 = m_b^2 \Delta z / 4R = m_b^2 / 4N_s$. Although we have not advanced a theory for this rule its functional form is not surprising and may be useful, particularly when high accuracy is required. When an inner scale is included, the Δz errors are still lower and, as the screen spacing approaches zero, the error I_{rms} is linearly proportional to Δz , in agreement with the results of Spivack and Uscinski¹⁶. The estimated rms intensity m does not change as Δz increases, even when $I_{rms} > m$. This is very similar to the behavior of the transverse sampling error shown in Fig. 1 and likewise implies that the error ΔI due to Δz is anticorrelated with the intensity itself. This behavior is consistent with the theoretical prediction of Spivack²⁷.

The spatial spectra of intensity and intensity error for two different Δz are shown in Fig. 5. Here we used a pure Kolmogorov spectrum and $m_b^2 = 1$. It is interesting that the error spectra are not white. The error spectra fall at higher wavenumbers such that they never exceed the spectrum of intensity by more than a factor of about 2.

The transverse sampling error for the extended medium simulation was estimated the same way as for the thin screen case using 128 screens for each simulation. The results are shown in Fig. 6 for two pure power-law turbulence spectra and a Kolmogorov spectrum with an inner scale $l_0 = 5\Delta s$. For the pure power-law cases, the best fit power-law for the thin-screen result [see Fig. 1] is overplotted showing remarkable agreement. The effect of the inner scale is also very similar to the thin screen result. The rms intensity m does not change with increasing Δs until $\Delta s > 2s_0$, as in the thin screen case, indicating that the anticorrelation of ΔI and I is similar.

The spatial spectra of intensity and intensity error due to transverse sampling are shown in Fig. 7 for a Kolmogorov spectrum with $m_b^2 = 1$. The error spectra are very similar to the thin screen spectra shown in Fig. 2, but are not directly comparable because we used a smaller m_b^2 for the extended medium simulation to reduce the computational burden.

The windowing error is investigated in an analogous manner to the thin screen case. For a pure power-law refractive index spectrum and uniform turbulence along the propagation path we can use the low wavenumber approximation given by¹⁷

$$\Phi_I(q) = 8\pi k^2 \Phi_n(q) \int_0^R dz \sin^2[q^2(R-z)/(2k)] \exp\{-D_P[\frac{q}{k}(R-z)(1+\alpha z/R)/(1+\alpha)]\}. \quad (29)$$

The variance error is then

$$\Delta m^2 = \frac{\alpha 2^{\alpha+2} \Gamma(1+\alpha/2) D_P(r_f)^2}{\pi \Gamma(1-\alpha/2)} \int_0^{2\pi\delta\theta_0 R/L} du_x \int_0^{2\pi\delta\theta_0 R/L} du_y \int_0^1 dt \times u^{-\alpha-2} \sin^2[tu^2 s_0^2 / (2r_f^2)] \exp[-u^\alpha t^\alpha (1+\alpha-\alpha t)/(1+\alpha)]. \quad (30)$$

As with the thin screen case, for fixed $D_P(r_f)$ or m_b^2 the windowing error is a function of the parameter $\theta_0 R/L$. In the limit of large L the exponential term and the sine term of Eq. (30) can be expanded. The leading order result is

$$\frac{\Delta m^2}{m_b^2} = \frac{\alpha(2+\alpha)(2\pi\delta r_f/L)^{4-\alpha} I(\alpha)}{6\pi\Gamma(1-\alpha/2)\cos(\alpha\pi/4)}. \quad (31)$$

The windowing error, the best fit power-law function, and the theoretical predictions of Eqs. (21) and (29) with $\delta = 0.65$ (the same value as for the thin screen case Fig. 3) are plotted in Fig. 8 for the pure Kolmogorov spectrum with $m_b^2 = 1.0$. The theoretical scaling law agrees with the simulation. However, the statistical fluctuations of the estimates for m^2 are much larger than for the thin screen case because fewer realizations could be calculated in a reasonable amount of time.

We can now estimate the total number of mesh points required in a uniform medium calculation. If the acceptable error is fixed then the number of points in the three dimensional mesh is $N_{p3} = N_{p2}R/\Delta z = N_{p2}N_S$ so $N_{p3} \propto (m_b^2)^{4/\alpha+1}$. This very rapid increase of N_{p3} with m_b^2 sets a hard limit on the strength of scattering which can be simulated with this technique.

7. Point Source in a Uniform Medium

The case of a point source in an extended medium cannot be analyzed simply by replacing the incident plane wave with a point source because of the periodicity implied by the use of the DFT. With an incident plane wave the radiation diverges from the axis only due to scattering. Thus one period will interfere with another by an overlap of $\approx \theta_o R$. However in the spherical geometry the radiation is naturally diverging so the overlap from adjacent periods is more severe. This problem has been approximated^{14,1} using a diverging Gaussian beam as the incident field. The average intensity in the observation plane is then a function of the radial distance from the beam propagation axis. The statistics of the intensity must be calculated in the observation plane using a small region in the center of the simulation and normalizing the results by the average intensity. This approach requires careful choice of the beam width so the approximation to a spherical wave is good, but the window is not any larger than necessary. Another approach, which we have used here, is to cast the split-step algorithm in a spherically diverging coordinate system (r, η_x, η_y) defined by $x = r\eta_x, y = r\eta_y$ for $\eta_{x,y} \ll 1$.

In this coordinate system the field is written with respect to a monochromatic spherical wave

$$F(\vec{s}, r, t) = f_s(\vec{\eta}, r) \exp[i(kr - \omega t)]/r. \quad (32)$$

The parabolic wave equation is then

$$\frac{\partial f_s}{\partial r} = \frac{i}{2kr^2} \left(\frac{\partial^2 f_s}{\partial \eta_x^2} + \frac{\partial^2 f_s}{\partial \eta_y^2} \right) + ikn(r\eta_x, r\eta_x, z)f_s. \quad (33)$$

This can be solved in free space ($n=0$) by Fourier transformation with respect to η . The transform variables are $\vec{\eta} = \vec{s}/r$ and $\vec{\beta} = \vec{q}r$. Then

$$f_s^t(\vec{\beta}, r) = f_s^i(\vec{\beta}, r_o) \exp[-i\beta^2(1/r_o - 1/r)/(2k)]. \quad (34)$$

This expression is used to propagate the field from one screen to the next. The transmittance of each screen is defined by its phase spectrum which is given by

$$\Phi_\phi(\vec{\beta}, r) = 2\pi k^2 \int_{r-\Delta r/2}^{r+\Delta r/2} z^{-2} \Phi_n(\vec{\beta}/z, q_z = 0) dz. \quad (35)$$

If $\Delta r \ll r$ then

$$\Phi_\phi(\vec{\beta}, r) = 2\pi k^2 \Delta r \Phi_n(\vec{\beta}/r, q_z = 0)/r^2. \quad (36)$$

For a pure power-law spectrum ($l_0 = 0$) and for $0 < \alpha < 2$, the strength of scattering m_b^2 , the coherence scale s_o and the structure function $D_S(\vec{s})$ are given by²²

$$m_b^2 = K_3(\alpha) D_S(r_f) \quad (37)$$

$$K_3(\alpha) = 2^\alpha \Gamma^3(1 + \alpha/2) \cos(\alpha\pi/4) / \Gamma(\alpha + 1) \quad (38)$$

$$D_S(\vec{s}) = (s/s_o)^\alpha = B_2(\alpha) k^2 C_n^2 R s^\alpha \quad (39)$$

$$B_2(\alpha) = 2^{1-\alpha} \Gamma(\alpha) \Gamma(1 - \alpha/2) \sin[(\alpha - 1)\pi/2] / [(\alpha + 1) \Gamma(1 + \alpha/2)]. \quad (40)$$

For the Kolmogorov exponent $B_2(5/3) = 1.09289$ and $K_3(5/3) = 0.454560$.

The point source simulation was tested against a reference using the same parameters and procedure as the plane-wave extended medium case. The intensity errors are plotted as a function of $\Delta z/R = 1/N_S$ in Fig. 9. For a fixed m_b^2 and pure power-law spectra, the error follows a power-law dependence with a similar exponent to that of the plane-wave case but the error at a given $\Delta z/R$ is about 4 times higher. For the Kolmogorov exponent the collection of intensity errors follows an approximate scaling rule $I_{rms}^2 = 4m_b^2 \Delta z/R = 4m_b^2/N_S$. When an inner scale is included, the errors are smaller and as the screen spacing approaches zero, I_{rms} is linearly proportional to Δz , which agrees with the results for the plane wave case.

The spatial spectra of the intensity and the intensity errors for two different values of Δz are shown in Fig. 10 for the Kolmogorov exponent $\alpha = 5/3$ and $m_b^2 = 1$. The intensity error spectra have a higher low-frequency contribution than the plane-wave case. However the dominant contribution to the total error variance is still from the higher wavenumber region.

The transverse sampling errors for the point source case are shown in Fig. 11 for two pure power-law turbulence spectra and a Kolmogorov spectrum with an inner scale $l_0 = 5\Delta s$. The best fit for the thin screen errors shown in Fig. 1 is overplotted. One can see that the fit to the pure power-law cases is again remarkably good. Clearly the errors due to transverse sampling are well described by the thin screen solution, both for plane and spherical waves. The effect of an inner scale is also very similar to that of the thin screen but this case is harder to scale. The estimated rms intensity m_{dec} is essentially constant for $\Delta s/s_o < 4$. The spectral density of the intensity sampling errors are shown in Fig. 12 for a Kolmogorov spectrum with $m_b^2 = 1$. As with the previous cases, the sampling error spectra are largest at high spatial frequencies and display characteristics of aliasing.

The windowing error is investigated in an analogous manner to the previous two cases. For a pure power-law refractive index spectrum and uniform turbulence along the propagation path, we use the low wavenumber approximation for the intensity spectrum^{17,26} and calculate the variance error by integrating over the first resolution element.

$$\Phi_I(q) = 8\pi k^2 \int_0^R dz \Phi_n(qR/z) \sin^2[q^2 z(R-z)/(2k)] \exp\{-D_S[q(R-z)/k]\} \quad (41)$$

$$\Delta m^2 = \frac{2^{\alpha+2} \alpha^2 (\alpha+1) \Gamma(1+\alpha/2) D_S(r_f)^2}{\pi \Gamma(1-\alpha/2)} \int_0^{2\pi\delta\theta_o R/L} du_x \int_0^{2\pi\delta\theta_o R/L} du_y \int_0^1 dt \times \\ t^\alpha u^{-\alpha-2} \sin^2[(1-1/t)u^2 s_o^2 / (2r_f^2)] \exp[-u^\alpha (1-t)^\alpha]. \quad (42)$$

For fixed $D_S(r_f)$ or m_b^2 the windowing error is a function of the parameter $\theta_o R/L$.

In the limit of large L the exponential term and the sin term of Eq. (42) can be expanded. The leading order result is

$$\frac{\Delta m^2}{m_b^2} = \frac{2\Gamma(1+\alpha)(2\pi\delta r_f/L)^{4-\alpha} I(\alpha)}{(\alpha-1)\Gamma(1-\alpha/2)\Gamma^2(1+\alpha/2)\cos(\alpha\pi/4)}. \quad (43)$$

The windowing error estimates from the simulations, the best fit power-law function, and the theoretical predictions of Eqs. (21) and (41) with $\delta = 0.75$ are plotted in Fig. 8 for the pure Kolmogorov spectrum with $m_b^2 = 1.0$. The theoretical scaling law agrees with the simulation at small $\theta_o R/L$. The higher terms of the series expansion for the intensity spectrum are required to predict the windowing error for larger $\theta_o R/L$.

8. Conclusion

The FFT split-step algorithm for wave propagation in random media is well-adapted to the case of an incident plane wave. It can be applied to the case of an incident spherical wave if a diverging spherical coordinate system is used. We find that the error scaling in the two cases is essentially the same. The numerical accuracy of the algorithm can be determined by the error scaling as a function of transverse sampling (Δs), longitudinal sampling (Δz), and transverse dimension or window (L). The sampling errors can be studied directly by resampling a reference calculation, so one can determine the rms error by comparing the resampled calculation with the reference. This allows one to find any of the statistics of the error, for example its spectral distribution. The windowing error is more difficult, and we have only been able to estimate its effect on the variance by integrating the intensity spectrum over a fraction δ of the spatial frequency bin around zero frequency. Unfortunately we cannot create a sample of the windowing error by comparing with a reference field, because of the periodicity of the window.

The transverse sampling error for power-law spectra as a function of $\delta s/s_o$ is exactly the same for the three cases tested, i.e. thin screen and uniform media with plane wave or spherical wave incident. It is well described as an aliasing error in the angular spectrum so steeper phase spectra have less sampling error than flatter spectra. Phase spectra which include an inner scale are particularly steep so they can be simulated with relaxed sampling. The spatial spectrum of the sampling error is characterized by maximum contribution at the high wavenumbers indicating a small spatial scale and aliasing.

The longitudinal sampling error is not properly described as an aliasing error although it is similar. It is clear these errors are primarily due to high frequency components because steeper power-law spectra have smaller errors as do spectra which include an inner

scale. The scaling with Δz is similar for plane wave and point source simulations, but the point source errors are 4 times higher. The spatial spectrum of the longitudinal sampling error is also concentrated at high wave-number but displays a high-frequency cutoff. The point-source error spectrum has a larger low-frequency component than the plane-wave case.

A theoretical expression for the Δz scaling of the field error has been given by Spivack and Uscinski¹⁶ when the random medium has finite derivatives. The Δz error determined from the simulations for the plane wave and point source agrees with this scaling when an inner scale is included. For a pure power-law spectrum we obtained a weaker scaling law, presumably because the finite derivative constraint was violated. Spivack²⁷ also calculated the $(\Delta z)^2$ dependence for the error of higher moments. This error scaling is difficult to verify because the estimation error of the higher moments is large^{28,29}. Thus many independent samples are required to produce accurate estimates and we were unable to confirm this scaling for the intensity variance or any higher moments.

A similar problem occurred in attempting to verify the theoretical model for the windowing errors in the intensity variance. For the thin screen simulation, shown in Fig. 3, it was easy to calculate many realizations of the field and the windowing error was accurately determined. For extended medium simulations, which are shown in Fig. 8, the errors are considerably larger. However, the windowing error does follow the predictions of our theoretical model.

When an inner scale is included the error scaling is not a simple power-law and the errors are less than for the pure power-law case because the high spatial frequency fluctuations of the medium and field are reduced. The error analysis presented here can be extended to any spectral model for the turbulence and finite beam propagation. It would be very valuable if the error in estimating the moments could be expressed in terms of the transverse sampling error and the Δz error since both of these errors can be accurately estimated with few calculations.

Acknowledgments

This work was partially supported by the National Science Foundation under grant ATM-82-09603 and the National Aeronautics and Space Administration Marshall Space Flight Center under Research Grant NAG8-253 (Michael J. Kavaya, Technical Officer).

References

1. S. M. Flatté, G. Wang, and J. Martin, "Irradiance variance of optical waves through atmospheric turbulence by numerical simulation and comparison with experiment," *J. Opt. Soc. Am. A* **10**, 2363-2370 (1993).
2. R. G. Frehlich, "The effects of global intermittency on wave propagation in random media," submitted to *Applied Optics*.
3. R. G. Frehlich and M. J. Kavaya, "Coherent laser radar performance for general atmospheric refractive turbulence," *Appl. Opt.* **30**, 5325-5352 (1991).
4. R. G. Frehlich, "Effects of refractive turbulence on coherent laser radar," *Appl. Opt.* **32**, 2122-2139, (1993)
5. W. A. Coles and J.P. Filice, "Dynamic spectra of interplanetary scintillations," *Nature* **312**, 251-254 (1985).
6. R. Buckley, R., "Diffraction by a random phase-changing screen: A numerical experiment," *J. Atmos. Terr. Phys.* **37**, 1431-1446 (1975).
7. C. L. Rino, "On the application of phase screen models to the interpretation of ionospheric scintillation data," *Radio Science* **17**, 855-867 (1982).
8. D. L. Knepp, "Multiple phase-screen calculation of the temporal behavior of stochastic waves," *Proc. IEEE* **71**, 722-737 (1983).
9. C. H. Liu and S. J. Franke, "Experimental and theoretical studies of ionospheric irregularities using scintillation techniques," *Radio Science* **21**, 363-374 (1986).
10. C. L. Rino and J. Owen, "Numerical simulations of intensity scintillation using the power law phase screen model," *Radio Science* **19**, 891-908 (1984).
11. C. Macaskill and T.E. Ewart, "Computer simulation of two-dimensional random wave propagation," *IMA J. Appl. Math.* **33**, 1-15 (1984).
12. J. P. Filice, "Studies of the microscale density fluctuations in the solar wind using interplanetary scintillations," PhD. thesis, Univ. Calif., San Diego, (1984).
13. J. M. Martin and S. M. Flatté, "Intensity images and statistics from numerical simulation of wave propagation in 3-D random media," *Appl. Opt.* **27**, 2111-2126 (1988).
14. J. M. Martin and Stanley M. Flatté, "Simulation of point-source scintillation through three-dimensional random media," *J. Opt. Soc. Am. A* **7**, 838-847 (1990).
15. J. Martin, "Simulation of wave propagation in random: theory and applications," in *Wave Propagation in Random Media (Scintillation)* Editors: V. I. Tatarskii, A. Ishimaru, and V. U. Zavorotny, SPIE Press and IOP Publishing, (1993)
16. M. Spivack and B. J. Uscinski, "The split-step solution in random wave propagation," *J. Comp. Appl. Math.* **27**, 349-361 (1989).
17. A. M. Prokhorov, F.V.Bunkin, K.S. Gochelashvily, and V.I.Shishov, "Laser irradiance propagation in turbulent media," *Proc. IEEE* **63**, 790-811 (1975).
18. R. G. Frehlich, R. G., "Laser scintillation measurements of the temperature spectrum in the atmospheric surface layer," *J. Atmos. Sci.* **49**, 1494-1509 (1992).
19. V. I. Tatarskii, *The Effects of the Turbulent Atmosphere on Wave Propagation*, "National Technical Information Service, Springfield, Va., (1971).
20. V. U. Zavorotnyi, "Strong fluctuations of electromagnetic waves in a random medium with finite longitudinal correlation of the inhomogeneities," *Zh. Eksp. Teor. Fiz.* **75**, 56-65 (1978). English, *Soviet Physics JETP* **48**, 27-31 (1978).

21. R. L. Fante, "Inner-scale size effect on the scintillations of light in the turbulent atmosphere," *J. Opt. Soc. Am.* **73**, 277-281 (1983).
22. R. G. Frehlich, "Intensity covariance of a point source in a random medium with a Kolmogorov spectrum and an inner scale of turbulence," *J. Opt. Soc. Am. A* **4**, 360-366 (1987).
23. W. A. Coles, R. G. Frehlich, B. J. Rickett, and J. L. Codona, "Refractive scintillation in the interstellar medium," *Astrophys. J.* **315**, 666-674 (1987).
24. R. Narayan and W. B. Hubbard, "Theory of anisotropic refractive scintillation: application to stellar occultations by neptune", *Astrophys. J.* **325**, 503-518 (1988).
25. S. M. Flatté, R. Dashen, W.H. Munk, K.M. Watson, and F. Zachariassen, *Sound Transmission Through a Fluctuating Ocean*, Cambridge University Press series on Mechanics and Applied Mathematics (1979).
26. J. L. Codona, D. B. Creamer, S. M. Flatté, R. G. Frehlich, and F. S. Henyey, "Solution for the fourth moment of waves propagating in random media," *Radio Science* **21**, 929-948 (1986).
27. Spivack, M., "Accuracy of the moments from simulation of waves in random media," *J. Opt. Soc. Am. A* **7**, 790-793 (1990).
28. N. Ben-Yosef and E. Goldner, "Sample size influence on optical scintillation analysis. 1: Analytical treatment of the higher-order irradiance moments," *Appl. Opt.* **27**, 2167-2177 (1988).
29. R. G. Frehlich, J. H. Churnside, "Statistical properties of estimates of the moments of laser scintillation" *J. Mod. Opt.* **36**, 1645-1659 (1989).

FIGURES

Fig. 1. Intensity error I_{rms} due to transverse sampling Δs for a plane-wave incident on a thin-screen. The phase spectrum for the calculations in the top panel is a pure power-law with exponent $\alpha = 1$ and that in the middle panel has $\alpha = 5/3$. The phase spectrum used in the lower panel is an atmospheric spectrum Eq. (2) with inner scale $l_0 = 5\Delta s$. The turbulence level for these spectra are described by the Born variance with zero inner scale Eq. (17). These are: $m_b^2 = 0.1$ (\circ), 1.0 (\square), and 10 (\diamond). The best fit power-law is plotted as a straight line on the upper two panels. The estimated rms intensity m_{dec} for $m_b^2 = 10$ is shown as a dashed line.

Fig. 2. Spatial spectra of intensity (\bullet) and intensity error due to transverse sampling (open symbols) for a plane-wave phase-screen simulation with ($N = 2048$, $\Delta s = r_f/64$). The spectrum was a pure Kolmogorov power-law with $m_b^2=10$. The intensity error spectra were calculated for $\Delta s = r_f/32$ (\circ) and $\Delta s = r_f/16$ (\square).

Fig. 3. The intensity variance m^2 (top panel) and the windowing error I_{rms} (bottom panel) for a plane-wave phase-screen simulation as a function of $\theta_o R/L$. The phase spectrum was a pure Kolmogorov power-law with $m_b^2=1$. The results of the simulation are marked with a (\bullet). The best fit power-law is drawn as a solid line and the theoretical model Eqs. (21) and (22) for $\delta = 0.65$ is drawn as a dashed line.

Fig. 4. The normalized intensity error due to longitudinal sampling Δz for a plane-wave extended medium simulation. The phase spectra were pure power-law spectra with $\alpha = 1$ (top) and $5/3$ (middle) and an atmospheric spectrum Eq. (2) with $l_0 = 5\Delta s$ (bottom). The turbulence levels (for zero inner scale) are marked $m_b^2 = 0.1$ (\circ), 1.0 (\square), and 10 (\diamond). The normalized rms intensity m/m_b for $m_b^2 = 10$ is shown as a dashed line.

Fig. 5. Spatial spectra of the intensity (\bullet) and intensity error due to longitudinal sampling Δz (open symbols) for a plane-wave extended medium simulation with ($N = 512$, $\Delta s = r_f/16$, $N_S = 128$). The phase spectrum was a pure Kolmogorov power-law with Born variance $m_b^2=1$. The error spectra were calculated for $N_S = 64$ screens (\circ) and 32 screens (\square).

Fig. 6. Intensity error I_{rms} due to transverse sampling Δs for a plane-wave extended medium simulation with ($N = 512$, $\Delta s = r_f/16$, $N_S = 128$). The phase spectra were a pure power-law with $\alpha = 1$ (top panel); $\alpha = 5/3$ (middle) and an atmospheric spectrum Eq. (2) with inner scale $l_0 = 5\Delta s$ (bottom). The turbulence level for these spectra are described by the Born variance with zero inner scale Eq. (25). These are: $m_b^2 = 0.1$ (\circ), 1.0 (\square), and 10 (\diamond). The best fit power-law from the thin screen simulations (Fig. 1) is plotted as a straight line on the upper two panels. The estimated rms intensity m_{dec} for $m_b^2 = 10$ is shown as dashed line.

Fig. 7. - Spatial spectra of intensity (\bullet) and intensity error due to transverse sampling (open symbols) for a plane-wave extended medium simulation with ($N = 512, \Delta s = r_f/16, N_S = 128$). The phase spectrum was a pure Kolmogorov power-law with Born variance $m_b^2=1$. The intensity error spectra were calculated for $\Delta s = r_f/8$ (\circ) and $\Delta s = r_f/4$ (\square).

Fig. 8. The normalized variance m^2 for plane-wave and point-source extended medium simulations as a function of $\theta_o R/L$. The phase spectrum was a pure Kolmogorov power-law with $m_b^2=1$. The best fit power-law models are drawn as solid lines and the theoretical expression are drawn as dashed lines. For the plane wave case, the theoretical model is given by Eqs. (21) and (30) with $\delta = 0.65$. For the point source case, the theoretical model is given by Eqs. (21) and (42) with $\delta = 0.75$.

Fig. 9. The normalized intensity error due to longitudinal sampling Δz for a point-source extended medium simulation. The phase spectra were a pure power-law with $\alpha = 1$ (top) and $5/3$ (middle) and an atmospheric spectrum Eq. (2) with $l_0 = 5\Delta s$ (bottom). The turbulence levels (for zero inner scale) are $m_b^2 = 0.1$ (\circ), 1.0 (\square), and 10 (\diamond). The estimated rms intensity m/m_b for $m_b^2 = 10$ is shown as a dashed line.

Fig. 10. Spatial spectra of the intensity (\bullet) and intensity error caused by longitudinal sampling Δz (open symbols) for a point-source extended medium simulation with ($N = 512, \Delta s = r_f/16, N_S = 128$). The phase spectrum was a pure Kolmogorov power-law with Born variance $m_b^2=1$. The error spectra were calculated for $N_S = 64$ screens (\circ) and 32 screens (\square).

Fig. 11. Intensity error I_{rms} due to transverse sampling Δs for a point-source simulation with ($N = 512, \Delta s = r_f/16, N_S = 128$). The spectra were a pure power-law spectrum with $\alpha = 1$ (top panel); $\alpha = 5/3$ (middle) and an atmospheric spectrum Eq. (2) with $l_0 = 5\Delta s$ (bottom). The turbulence level for these spectra are described by the Born variance (with zero inner scale Eq. (37)). These are: $m_b^2 = 0.1$ (\circ), 1.0 (\square), and 10 (\diamond). The best fit power-law from the thin screen simulation (Fig. 1) is plotted as a straight line on the upper two panels. The estimated rms intensity m_{dec} for $m_b^2 = 10$ is shown as a dashed line.

Fig. 12. Spatial spectra of intensity (\bullet) and intensity error due to transverse sampling (open symbols) for a point-source extended medium simulation with ($N = 512, \Delta s = r_f/16, N_S = 128$). The phase spectrum was a pure Kolmogorov power-law with Born variance $m_b^2=1$. The intensity error spectra were calculated for $\Delta s = r_f/8$ (\circ) and $\Delta s = r_f/4$ (\square).

Figure 1

Thin Screen Decimation Error

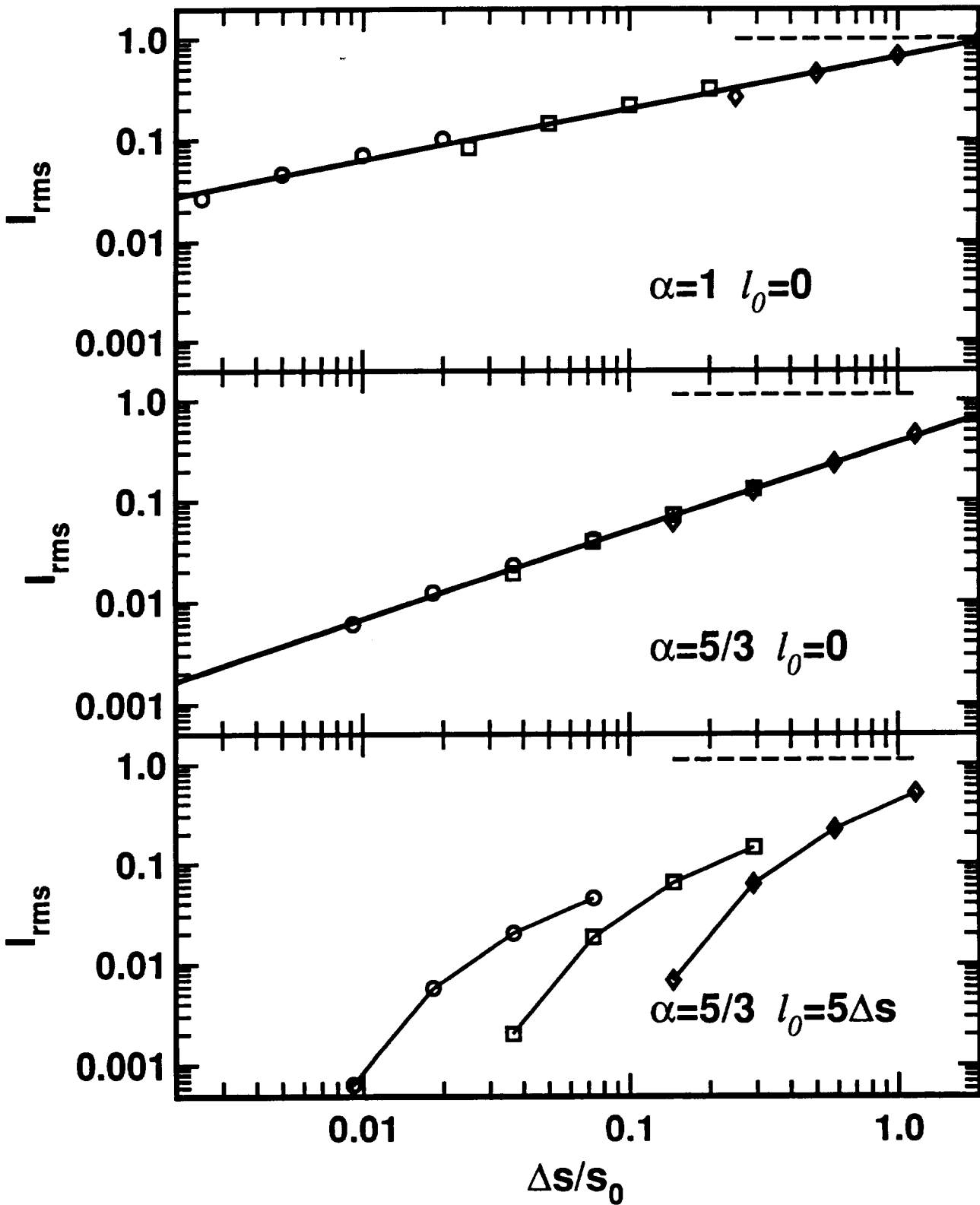


Figure 2

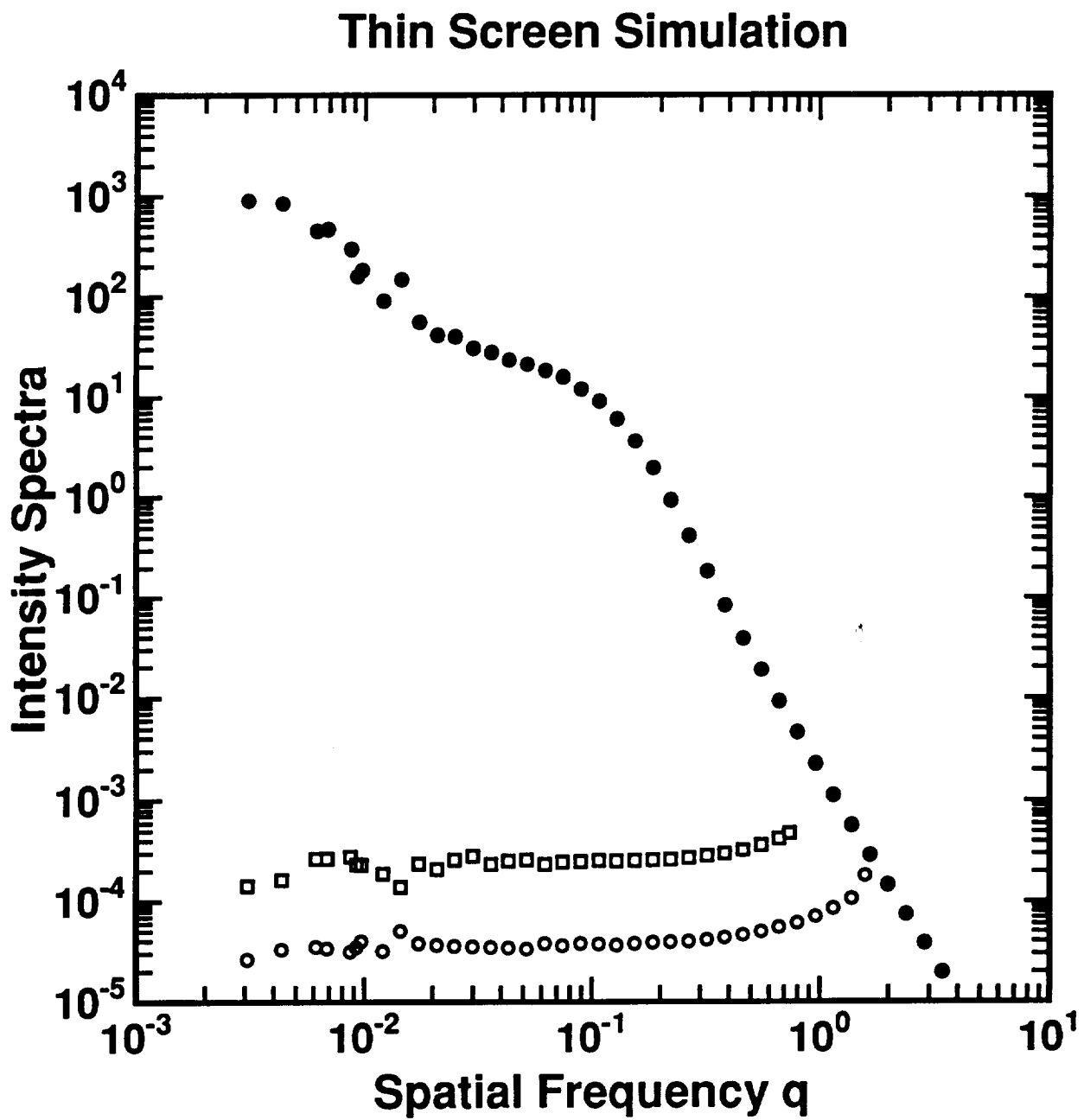


Figure 3

Kolmogorov Thin Screen Simulation

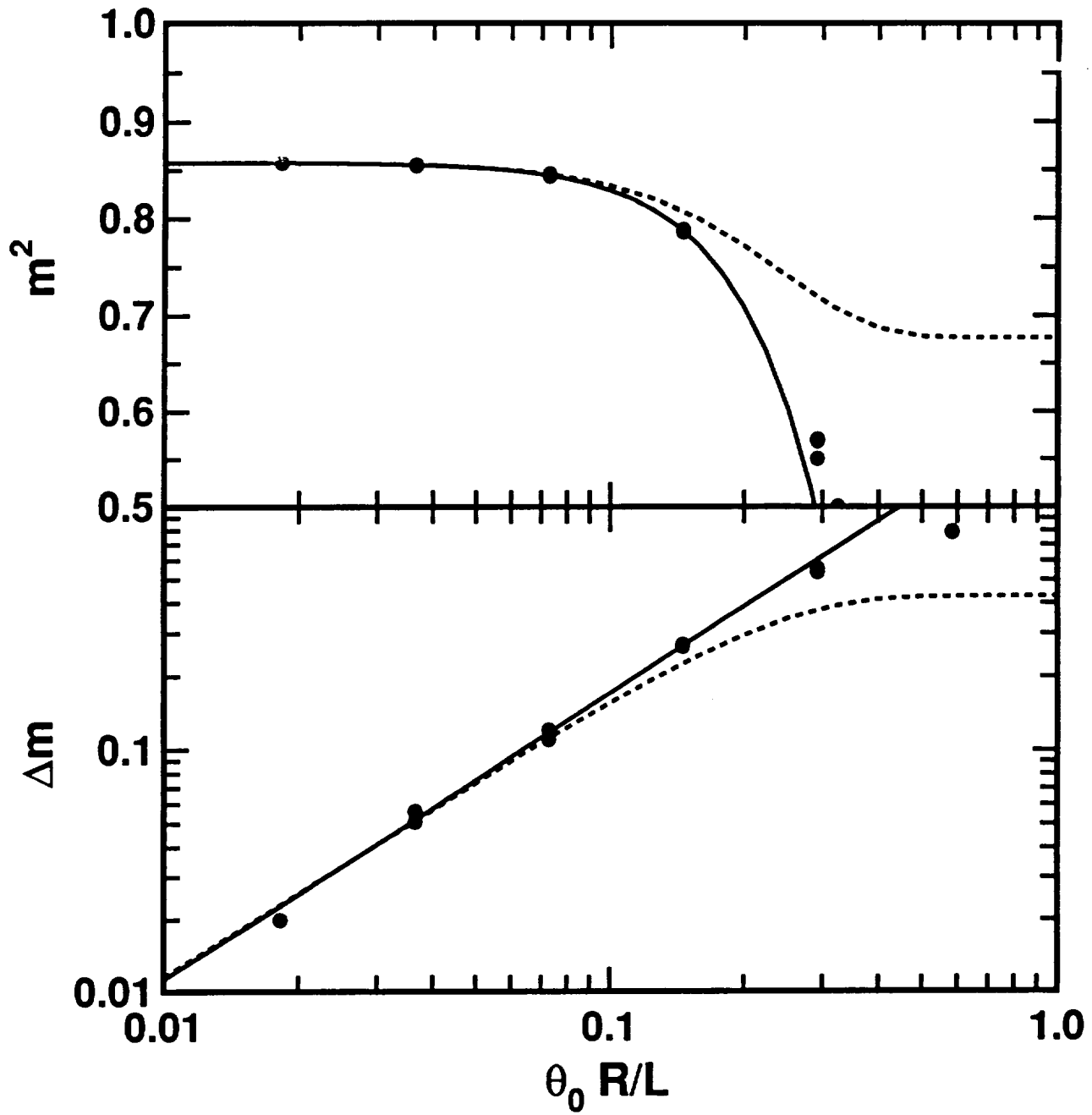


Figure 4

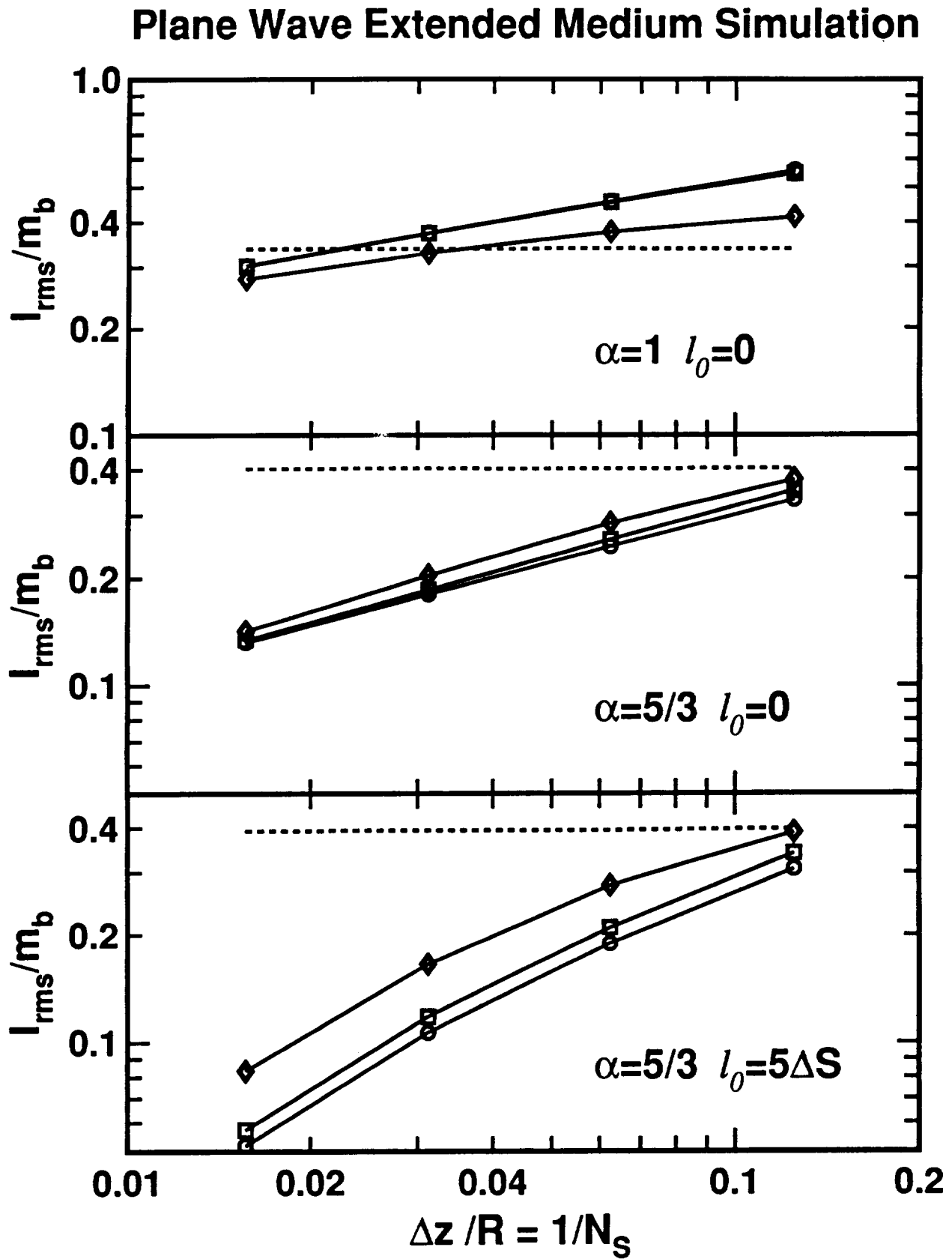


Figure 5

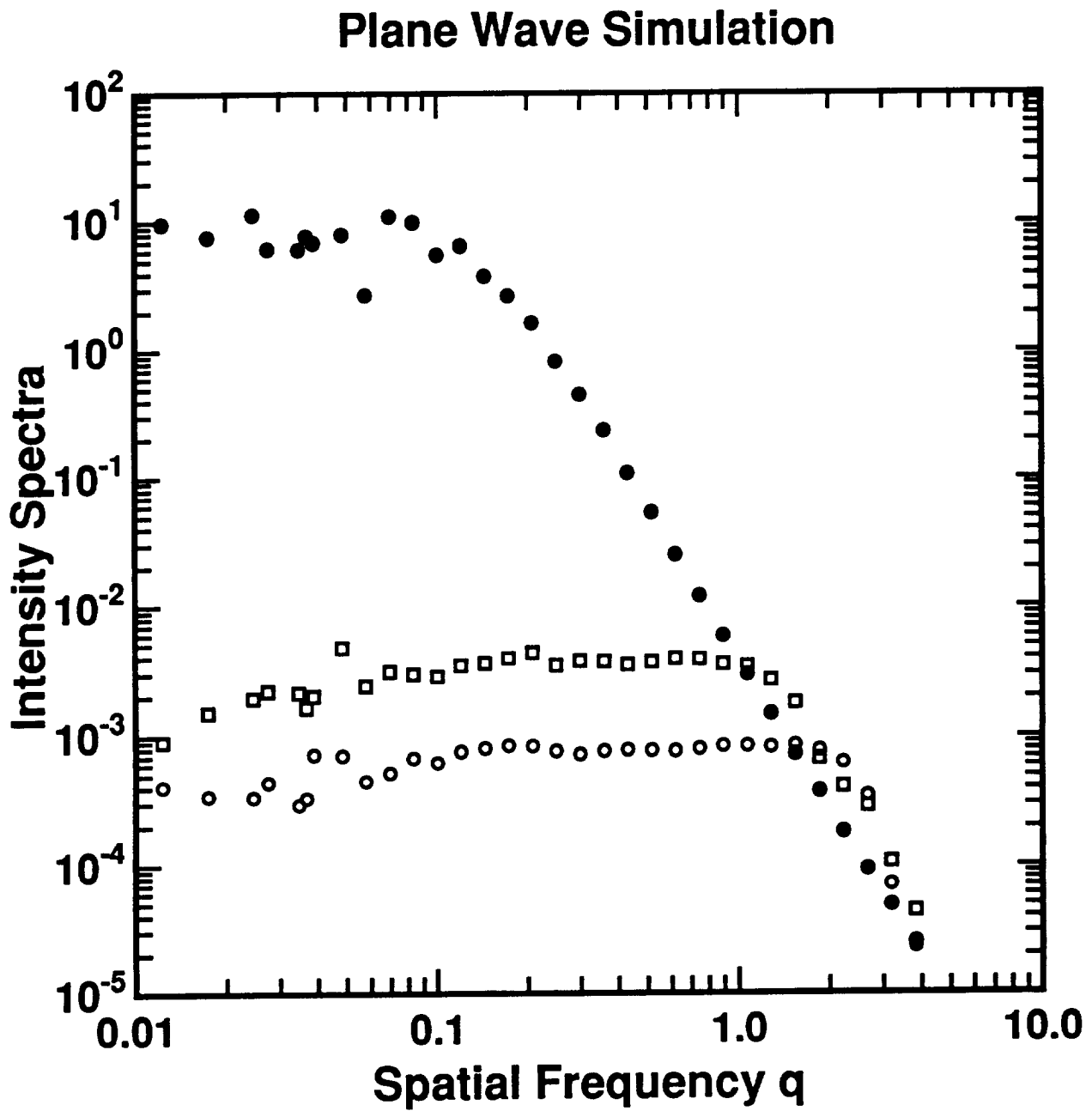


Figure 6

Plane Wave Decimation Error

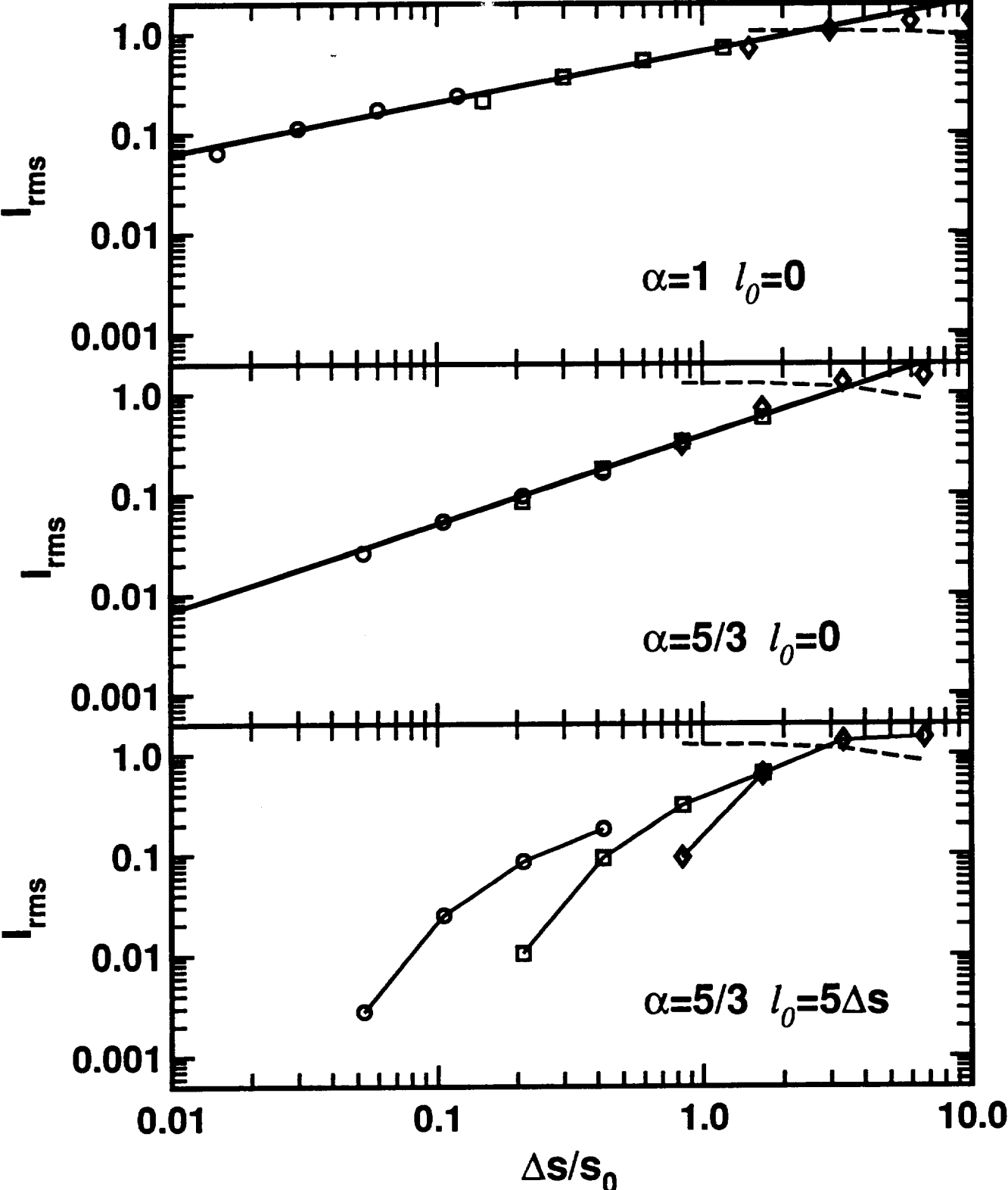


Figure 7

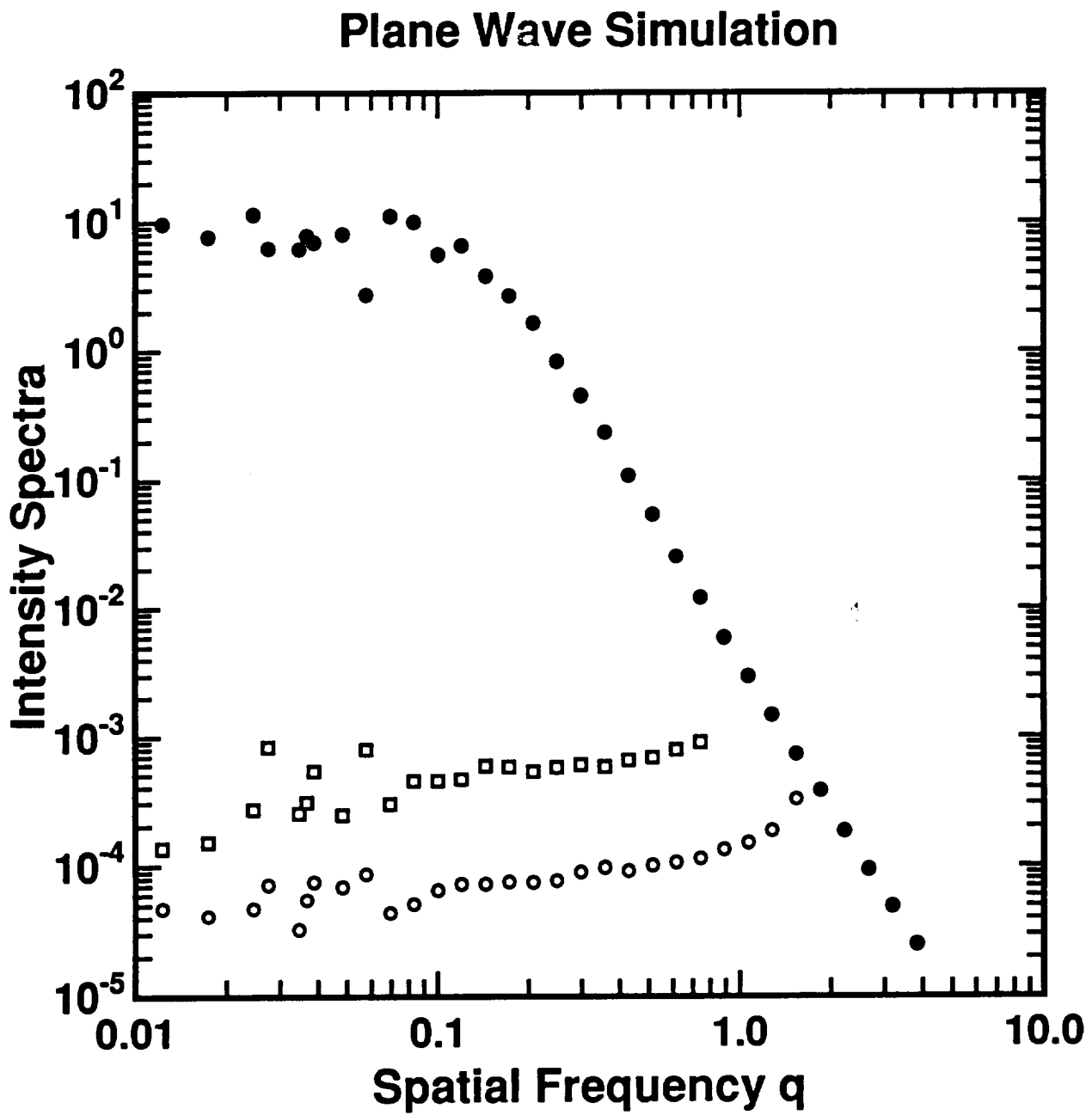


Figure 8

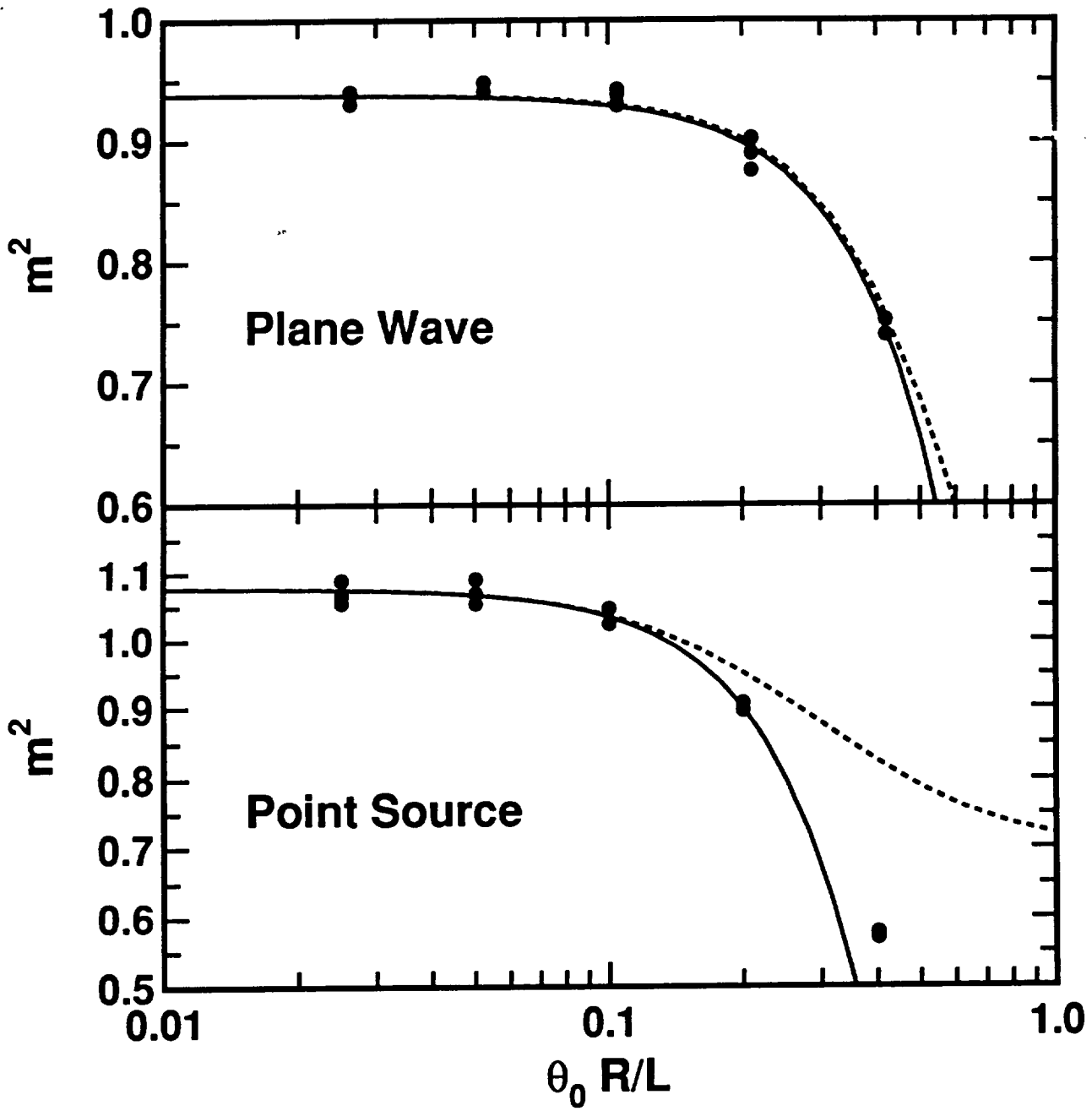


Figure 9

Point Source Simulation

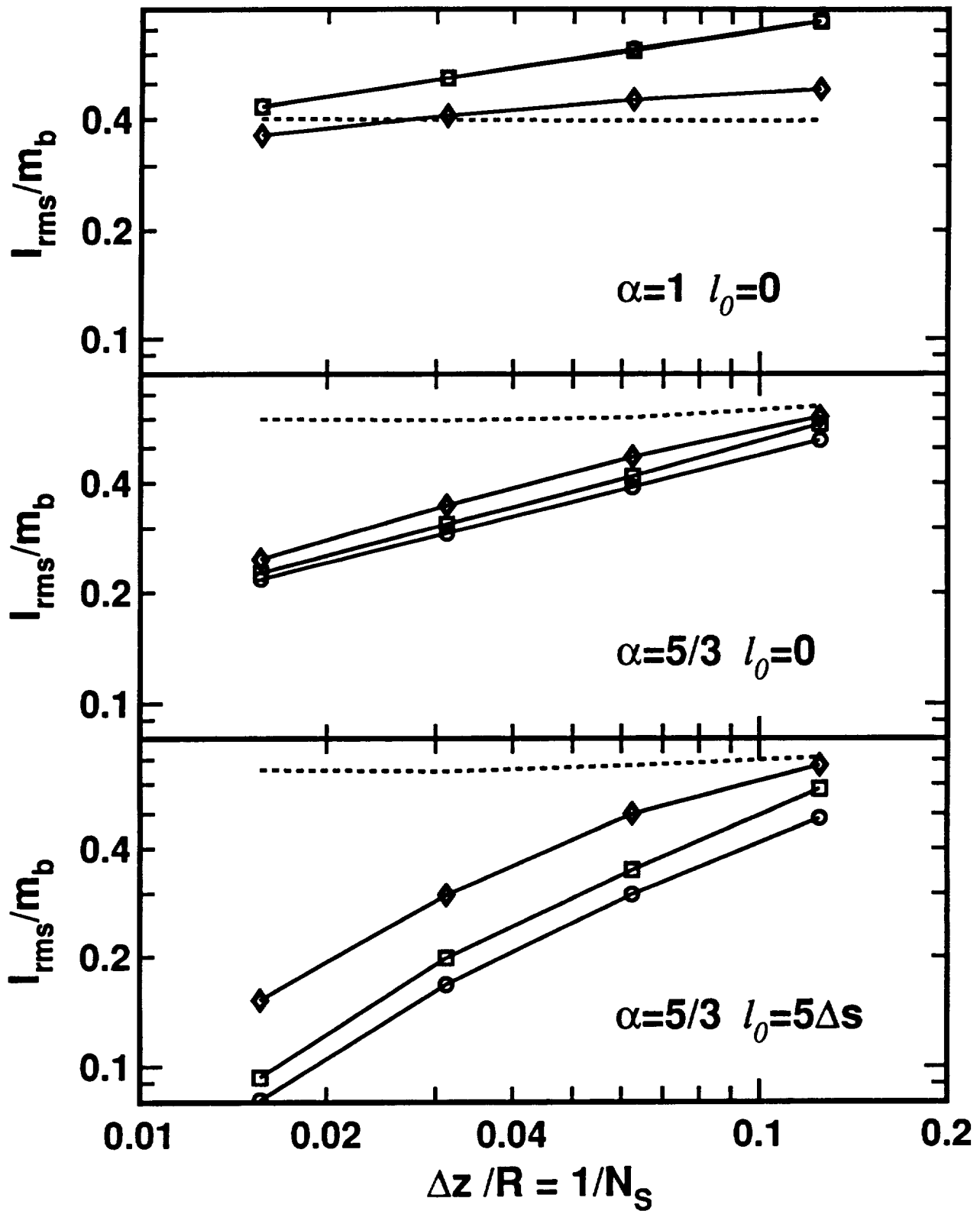


Figure 10

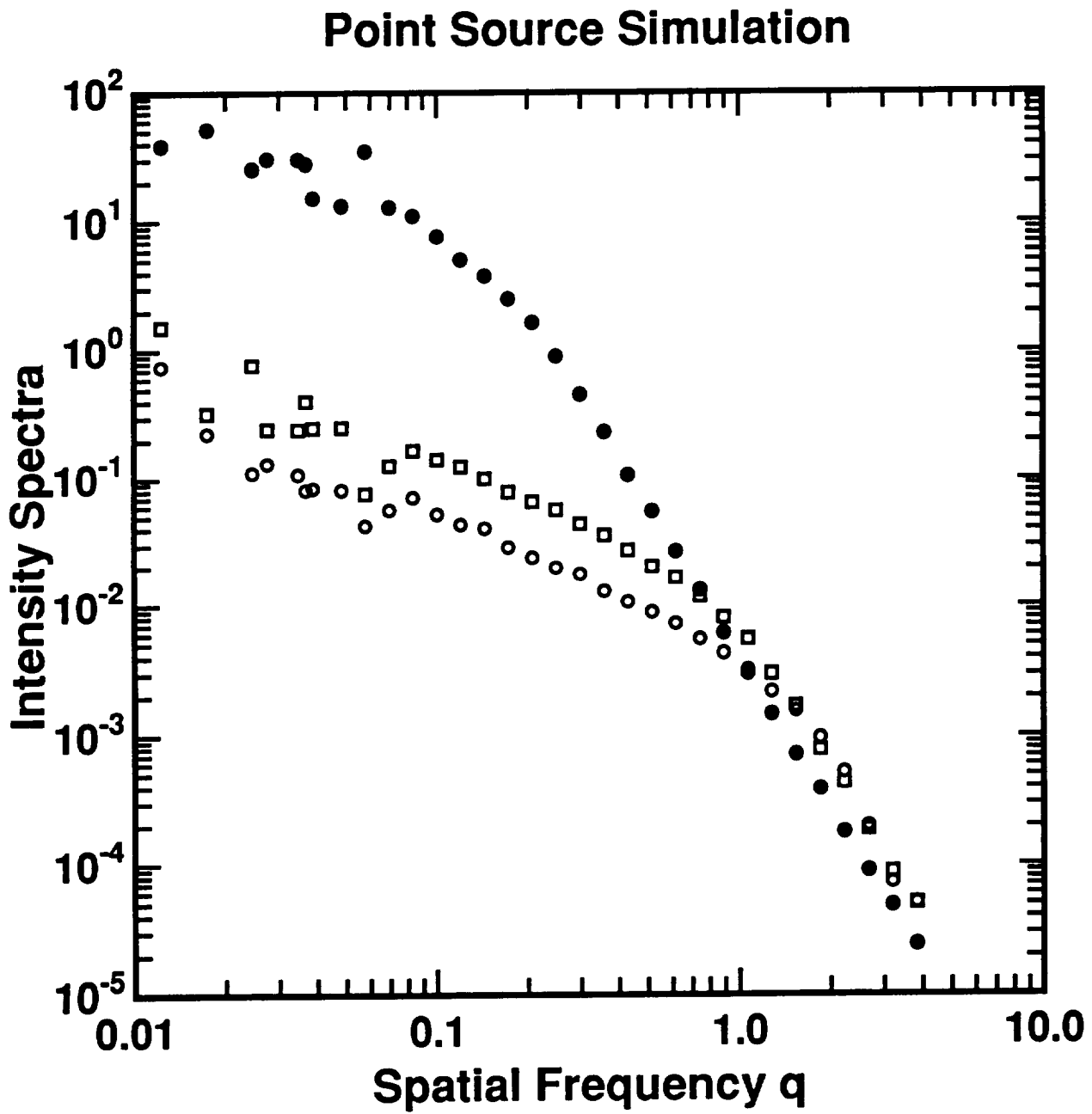


Figure 11

Point Source Decimation Error

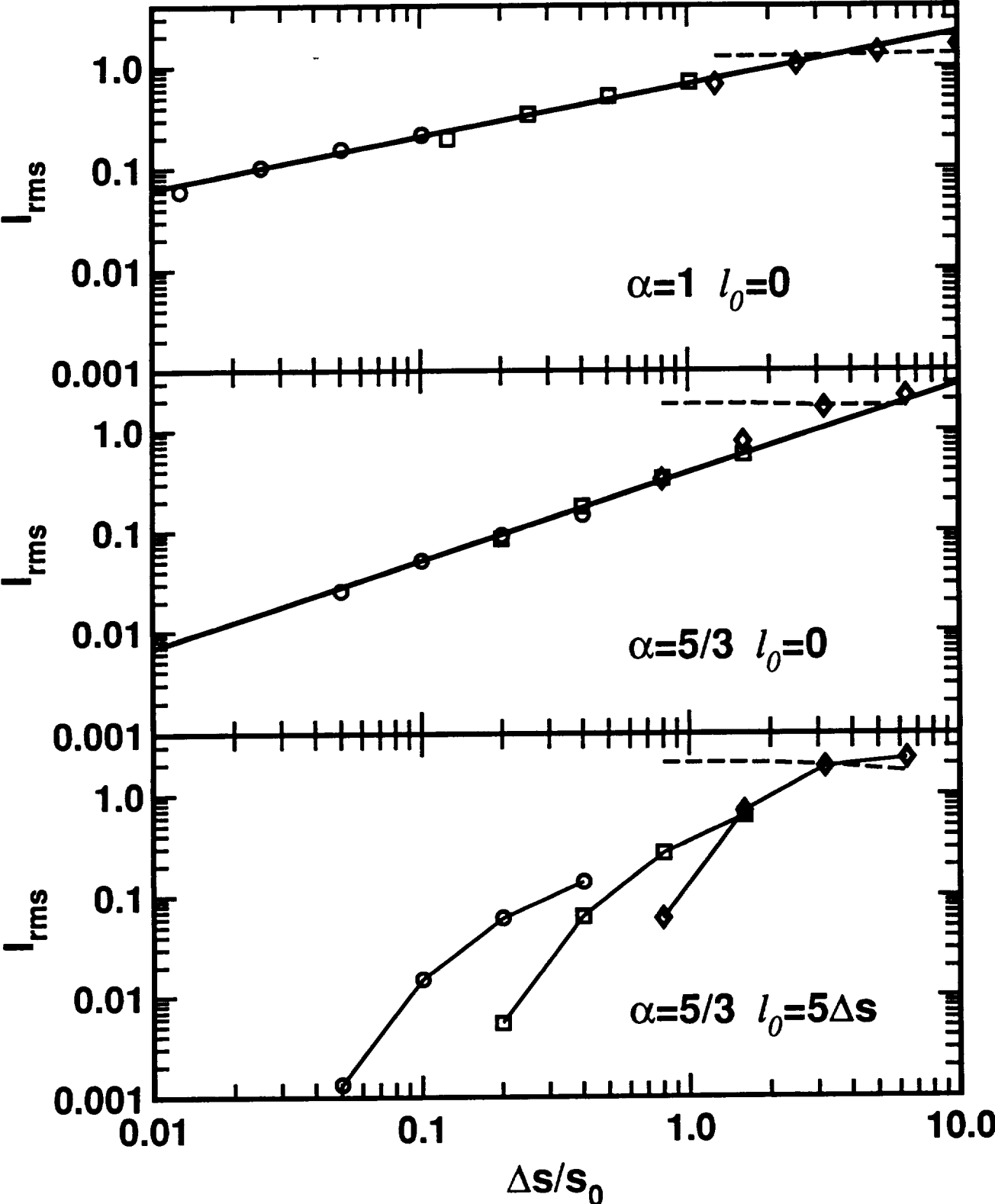


Figure 12

